Microscopy and Microanalysis, 2023, **00**, 1–10
https://doi.org/10.1093/micmic/ozac029

Microscopy AND Microanalysis

Original Article

Cryo-EXLO Manipulation of FIB Specimens for Cryo-TEM

Lucille A. Giannuzzi[1,*], Michael Colletta[2], Yue Yu[2], Lena F. Kourkoutis[2,3], Andrew D. Iams[4], Kyle Beggs[5], and Alain J. Kassab[5]

[1]*EXpressLO LLC, 5483 Lee St Unit 12, Lehigh Acres, FL 33971, USA*
[2]*Applied and Engineering Physics, Cornell University, Ithaca, NY 14853, USA*
[3]*Kavli Institute at Cornell for Nanoscale Science, Cornell University, Ithaca, NY 14853, USA*
[4]*Materials Science & Engineering, The Pennsylvania State University, University Park, PA 16802, USA*
[5]*Centecorp LLC, 147 Parsons Rd, Longwood, FL 32779, USA*

***Corresponding author:** Lucille A. Giannuzzi, E-mail: lucille.giannuzzi@expresslo.com

Abstract

This work describes cryogenic *ex situ* lift out (cryo-EXLO) of cryogenic focused ion beam (cryo-FIB) thinned specimens for analysis by cryogenic transmission electron microscopy (cryo-TEM). Steps and apparatus necessary for cryo-EXLO are described. Methods designed to limit ice contamination include use of an anti-frost lid, a vacuum transfer assembly, and a cryostat. Cryo-EXLO is performed in a cryostat with the cryo-shuttle holder positioned in the cryogenic vapor phase above the surface of liquid N_2 (LN2) using an EXLO manipulation station installed inside a glove box maintained at < 10% relative humidity and inert (e.g., N_2 gas) conditions. Thermal modeling shows that a cryo-EXLO specimen will remain vitreous within its FIB trench indefinitely while LN2 is continuously supplied. Once the LN2 is cut off, modeling shows that the EXLO specimen will remain vitreous for over 4 min, allowing sufficient time for the cryo-transfer steps which take only seconds to perform. Cryo-EXLO was applied successfully to cryo-FIB-milled specimen preparation of a polymer sample and plunge-frozen yeast cells. Cryo-TEM of both the polymer and the yeast shows minimal ice contamination with the yeast specimen maintaining its vitreous phase, illustrating the potential of cryo-EXLO for cryo-FIB-EM of beam-sensitive, liquid, or biological materials.

Key words: cryo-lift out, cryo-FIB, cryo-EXLO, cryo-TEM, *ex situ* lift out

Introduction

The 2017 Nobel prize in chemistry recently awarded to Dubochet, Frank, and Henderson, for developing cryo-transmission electron microscopy (cryo-TEM) methods for high-resolution structure determination of biomolecules is a testament to cryo-TEM's importance. Cryo-TEM of biological samples requires the area of interest to be frozen in a layer of amorphous or vitreous ice which is thin enough to be electron transparent. Vitreous ice is required for cryo-TEM since crystalline ice produces diffraction contrast that can obscure signal from the material of interest. In addition, the nucleation and growth of ice crystals can damage or deform molecules within biological samples. Cryo-plunge freezing techniques by Dubochet et al. revolutionized cryo-EM analysis of assemblies of single particles and for cryo-tomographic studies of single objects (Doubochet & McDowall, 1981). For cryo-TEM single particle analysis, a suspension of particles is deposited onto a lacey or holey carbon-coated TEM grid, blotted to remove excess liquid, cryo-plunged into liquid ethane (or liquid nitrogen) to obtain fast cooling rates to form a thin electron transparent vitreous layer and cryo-transferred into a cryo-TEM holder for imaging in a cryo-TEM. High-pressure freezing is needed for cryo-TEM of thicker (> 200 μm) samples to ensure that vitreous ice is maintained throughout the large sample (Giddings et al., 2001). These thicker samples may be subsequently sectioned into slices using cryo-microtomy and then micromanipulated to a carbon-coated TEM grid (Ladinsky, 2010). However, samples sectioned with cryo-microtomy suffer from knife chatter artifacts (i.e., structural deformation) and the preparation and analysis of many tens of slices may be necessary to find the desired region of interest.

The use of cryogenic focused ion beam (cryo-FIB) milling and cross-sectioning was first verified on yeast cells (Heymann et al., 2006). Since then the use of cryo-FIB specimen preparation has been successfully applied to cryo-TEM sample preparation, negating cryo-microtomy artifacts (Marko et al., 2006; Ladinsky, 2010; Antoniou et al., 2012; Rigort et al., 2012; Rubino et al., 2012; Hsieh et al., 2014; Zachman et al., 2017; Schaffer et al., 2018; Zachman et al., 2018). These cryo-FIB methods have also been extended to beam-sensitive engineering materials, liquid/solid interfaces, and other materials of interest in battery research and the physical sciences (Antoniou et al., 2012; Zachman et al., 2017; Li et al., 2018; Zachman et al., 2018; Choudhury et al., 2019). In this paper, we present a novel manipulation method of cryo-FIB prepared specimens for cryo-TEM analysis. First, we will review FIB manipulation methods.

Background on Cryo in situ *Lift Out (Cryo-INLO)*

Cryo-FIB INLO requires the use of an INLO tip configured with a cryostat such that the tip can be maintained at cryogenic temperatures to retain the vitreous phase during sample extraction (i.e., lift out) from the bulk sample which is also maintained at cryogenic temperatures held on a cryo-stage in the FIB (Antoniou et al., 2012; Rubino et al., 2012;

Received: May 31, 2022. **Revised:** August 10, 2022. **Accepted:** August 24, 2022

Zachman et al., 2017; Schaffer et al., 2018; Zachman et al., 2018; Klumpe et al., 2021). There are numerous complex steps required for cryo-FIB INLO: (i) the cryo-tip must be attached to the sample using either Pt deposition, ice attachment, friction-assisted phase changes, redeposition sputtering, or via direct gripping so that the sample can be removed from the bulk. It can be difficult to keep the cryo-sample and the cryo-probe tip at exactly the same temperature which results in thermal drift between the two as they touch. This thermal drift creates challenges for the attachment of the sample to the probe which must remain stable for several minutes during the deposition/attachment process. Instabilities caused by thermal drift can result in breakage and failure at the sample/probe interface. (ii) Once the probe is secured to the sample, the sample is FIB milled free from its trench and (iii) the probe/sample is retracted lifting out the sample. (iv) A metallic half-grid, also maintained at cryogenic temperatures on the cryo-stage, is positioned in the field of view, the probe/sample is brought back in and (v) attached to the half-grid (using similar attachment methods as above). Once again, thermal expansion and temperature differences can cause issues with sample attachment to the grid, resulting in the possibility of failure. (vi) The cryo-probe is FIB milled away (or ungripped) from the sample and the probe is retracted. (vii) The sample is then FIB milled to electron transparency. (viii) Then the grid sample carrier is cryo-transferred from the FIB (vii) to a cryo-TEM holder and loaded into the microscope for cryo-TEM imaging.

Cryo-INLO offers the same sample advantages as ambient INLO. That is, lift out can occur anywhere on the sample surface and the small sample profile allows for greater tilt flexibility for TEM-tomography. However, these problematic, complex, and time-consuming cryo-FIB INLO steps may require several tens of minutes to hours to complete successfully. This occupies the FIB for the better part of a day which bottlenecks the process of performing cryo-TEM and reduces access to the FIB for other tasks. A recent publication detailed specific times for all cryo-FIB milling and cryo-INLO manipulation steps (Parmenter & Nizamudeen, 2021). The cryo-INLO steps denoted can take up to 60 min to accomplish, with the entire cryo-FIB milling and cryo-INLO process consuming the majority of a workday. Thus, INLO methods requiring cryo-manipulation of FIB-prepared samples *inside* the FIB chamber result in numerous and complex steps, leading to poor success rates generating perhaps only one useable sample per day, ultimately increasing the cost per sample. This time-intensive process also ties up the FIB for potential other uses. Thus, this work focuses on fast, easy, and cost-effective implementation of cryogenic *ex situ* lift out for cryo-TEM.

Background on Ambient ex situ Lift Out (EXLO)

Historically, EXLO was the first lift out method developed for materials in ambient conditions, and thus, publications from the late 1990s and early 2000s refer to this as simply lift out. These early FIB milling techniques not only demonstrated that virtually *any* material could be FIB milled, but also demonstrated that *any* material could be *ex situ* manipulated (Giannuzzi et al., 1997; Giannuzzi & Stevie, 1999; Stevie et al., 2001; Ferryman et al., 2002; Giannuzzi et al., 2005; Giannuzzi et al., 2015). The FIB milling steps used for INLO are like those for EXLO. The primary difference is that the specimen is FIB milled to the desired thickness after FIB undercutting (which also removes any redeposited FIB artifacts) and milled so that the lamella specimen remains inside the FIB-milled trenches, and is supported by and touching the trench walls (see example Si EXLO specimen in Fig. 1a). The bulk sample containing the specimen(s) is then removed from the FIB and positioned onto a micromanipulator station consisting of a light optical microscope and micromanipulator system (Giannuzzi et al., 2015). A solid glass probe pulled to ~1 μm at its end is then positioned to lift out or pick up the sample and place it on a carbon, holey carbon TEM grid, or slotted grid for TEM analysis. A native glass probe can be used or the glass can be metallized to avoid unwanted excessive electrostatic forces, e.g., between a non-conductive glass probe and non-conductive specimen (Giannuzzi et al., 2015; Giannuzzi, 2017). In addition, EXLO samples can be used for correlative analyses using other microscopy or surface science methods (Stevie et al., 2001; Ferryman et al., 2002).

The dimensions of a typical EXLO sample for cryo-TEM might be 10–20 μm long × 5–10 μm wide/deep × 300 nm (or less) in thickness. The entire specimen length may be FIB milled or a small window portion of the entire specimen length can be preferentially FIB thinned. EXLO specimens can also be thinned after lift out when manipulated to specially designed slotted grids (Giannuzzi et al., 2015), albeit with an additional transfer step. An example of a 20 μm long ambient silicon EXLO specimen is shown in the ion-induced secondary electron FIB image in Figure 1a. 3D-printed polymer lift out samples can be used to teach and train users in the EXLO (or INLO) process (Giannuzzi et al., 2019*b*). These samples are printed to a thickness of 1 μm with 2-photon polymerization of liquid photoresist and an EXLO-ready sample is shown in Figure 1b.

Years ago, it was assumed that the mechanism of attachment of a specimen to the glass probe with EXLO was via electrostatic attraction. However, it was found that Van der Waals forces were the predominant attachment force for the successful manipulation of EXLO specimens (Giannuzzi et al., 2015). Van der Waals forces for a silicon sample attracted to a glass probe in air were found to be *~12 orders of magnitude larger* than the force of gravity acting on the sample. The Haymaker material constant in the Van der Waals force equation (Giannuzzi et al., 2015) varies by only 2 orders of magnitude across the entire periodic table; hence, Van der Waals forces may still be greater than 10 orders of magnitude larger than the force of gravity for any material at these dimensions. The fact that EXLO has been applied to so many different material types is borne out by adhesion physics as they are now understood. In addition, sample shape is irrelevant for these manipulations if sufficient surface area exists between the probe and sample. Indeed, EXLO has also been used to manipulate powders, fibers, and particulates for analyses (Ghassemi et al., 2017; Giannuzzi et al., 2019*a*). Work on Van der Waals forces also predicts that samples up to several hundred micrometers or more may be manipulated, and indeed, this has been verified (Giannuzzi et al., 2016).

It is well known that the EXLO process is fast and reproducible. In addition, the EXLO process is also easy to teach and master. Figure 1c shows a subset of more than 60 3D-printed polymer samples like those in Figure 1b, EXLO manipulated by both veteran and novice users of EXLO performed on and off over a period of ~24 h. Veteran users averaged a manipulation time of 1:05 (minutes) while novice users averaged a manipulation time of 2:51 (minutes) after receiving a brief

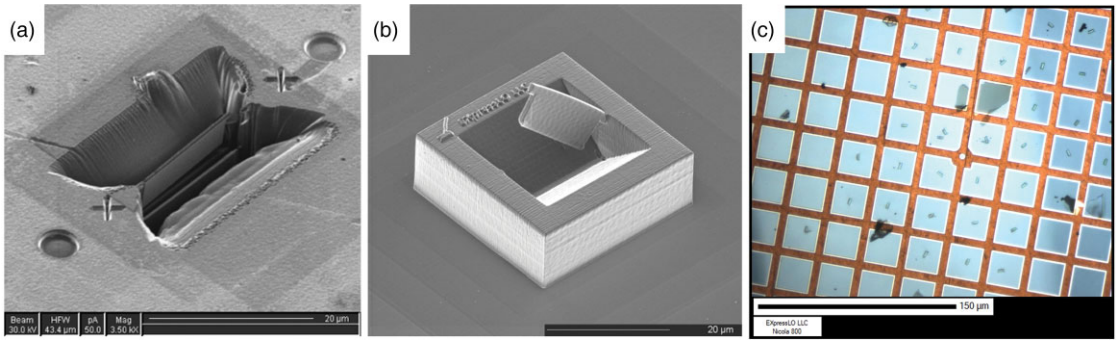

Fig. 1. (**a**) FIB-milled EXLO ready Si specimen. (**b**) 1 μm thick 3D-printed polymer practice lift out sample, FIB milled free and ready for EXLO. (**c**) 3D-printed samples EXLO manipulated to a carbon-coated EM grid and imaged in a light optical microscope.

few minutes' explanation and demonstration of the process. Thus, the number of samples that can be manipulated with EXLO in a timely and reproducible manner cannot be matched using INLO methods, as it can take a new user several hours to days to successfully manipulate their first ambient sample using INLO successfully. Cryo-INLO methods take even longer to master and accomplish. Thus, to better handle artifact-free cryo-TEM FIB specimens, we present a fast, easy, reproducible, and cost-effective cryo-FIB *ex situ* lift out (cryo-EXLO) sample handling and micromanipulation method for cryo-TEM.

Experimental Methods

We configured a conventional EXpressLO Nicola 640 lift out station with two hydraulic micro-manipulators and installed it inside a custom Coy glove box to keep the relative humidity less than 10% (details in the schematic diagram in Fig. 2). To reduce ice contamination during the EXLO process, the glove box was also periodically backfilled with up to 22 psi of nitrogen gas. Metallized glass probes were used for the cryo-EXLO manipulation processes. After probes were pulled to a fine tip, they were dipped in hobby India ink (e.g., carbon particles in colloidal suspension) and air dried to provide a conductive outer tip surface (Giannuzzi, 2017). Glass pulled tips can also be sputter-coated to yield a conductive outer surface (Giannuzzi et al., 2015). Metallized glass tips are preferred over metal tips typically used for INLO since they will not deform and can flex considerably without breaking.

An FEI (now Thermo Fisher Scientific) Strata 400S (Ga^+ ion) FIB SEM was used for all cryo-FIB milling steps. A Quorum PP3010T cryo stage and transfer system were used to maintain cryogenic temperatures during the FIB milling and transfer steps. The Quorum prep stage was maintained at −175°C. Inside the FIB SEM, the cryo-stage was maintained at −165°C while the anti-contaminator was maintained at −190°C.

To optimize the cryo-FIB time usage, several polymer specimens within a 3D-printed array of specimens were thinned to electron transparency (~300 nm thick) in ambient (e.g., non-cryo) conditions on a Thermo Fisher Scientific Scios (Ga^+ ion) FIB SEM in advance of access to the cryo-FIB. The pre-thinned 3D-printed polymer samples on a silicon substrate were attached to the cryo-FIB shuttle holder using carbon tape and transferred into the cryo-FIB via the usual Quorum preparation transfer station and load lock. The remaining material tabs for each polymer specimen were cryo-FIB milled free as needed and the samples were then cryo-transferred for cryo-EXLO.

Yeast cells in solution were deposited on a carbon-coated TEM grid and plunge-frozen in a mixture of liquid ethane and propane cooled by liquid nitrogen (LN2). Plunge-freezing equipment was readily accessible in our lab and others have shown that thin (< 20 μm) layers of cells can be successfully vitrified (Giddings et al., 2001). Note also that high-pressure frozen samples could also be used for the cryo-EXLO methods described below. The grids with plunge frozen yeast cells were held in place via a screw and clip mechanism on the cryo-FIB shuttle holder under LN2 using the Quorum slusher station and transferred into the preparation stage and load lock for metal sputter coating prior to full insertion into the cryo-FIB stage. The LN2 slusher station is used to mount the yeast cells onto the cryo-shuttle holder and provides a vacuum transfer mechanism via a rod attached to the shuttle for transferring the shuttle holder into the intermediate preparation chamber and then ultimately onto the cryo-FIB cold stage. The anti-frost lid was closed during the transfer steps, and opened during the sputter coating and the cryo-FIB milling steps. A suitable region of the yeast cells was identified, and a thick (~2 μm) layer of organometallic Pt was deposited and cured with the ion-beam as described earlier (Hayles et al., 2007). A thick Pt layer is necessary to reduce electrostatic charge issues and also reduces curtaining artifacts during cryo-FIB milling. Four EXLO yeast specimens were cryo-FIB prepared in < 4 h with final dimensions of ~20 μm × 7 μm × 300 nm. We used an assembly-line method to FIB mill the specimens, milling the same type of pattern on each specimen before lowering the beam current for the next FIB milling step. We optimized the cryo-FIB milling steps and times and used nominal FIB beam currents of 6.5 nA to mill the initial large trenches, 2.8 nA to further thin the specimen, 0.9 nA for additional thinning and the U-shaped undercut mill, followed by smaller beam currents as needed (e.g., 0.46, 0.28, 93 pA) to achieve the desired thickness. It should be noted that these beam currents are a factor of 6× or more larger than those reported for trenching and final milling of cryo-INLO specimens (Parmenter et al., 2016; Schaffer et al., 2019). As will be shown, our combined cryo-FIB milling methods plus cryo-EXLO saves considerable time compared to cryo-INLO.

For both the polymer and the yeast cryo-EXLO methods, C-Flat™ grids were pre-clipped in autogrids for easy and direct transfer after cryo-EXLO to an autoloader for analysis with a Thermo Fischer Scientific Arctica cryo-TEM. The grids were pre-processed at room temperature in a GloQube plasma

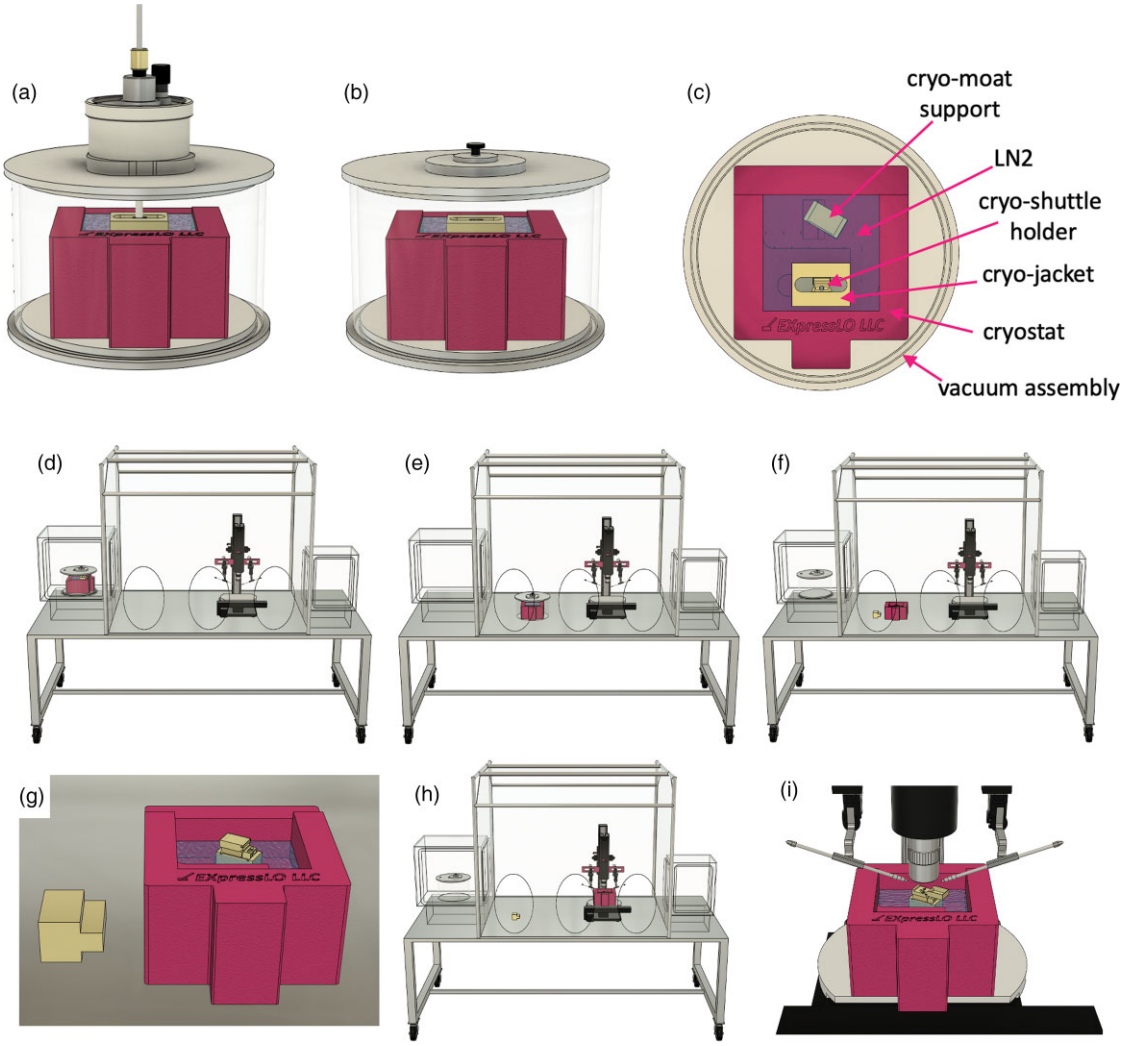

Fig. 2. Schematic diagram of the cryo-transfer process from the cryo-FIB transfer rod to the cryostat vacuum assembly. (**a**) The cryo-shuttle holder is transferred to the cryo-jacket inside the cryostat. (**b**) The transfer rod is removed and the cryostat is covered with a lid to evacuate the assembly. (**c**) A top down view of the cryo-shuttle holder positioned inside the cryo-jacket with parts labeled. (**d**) The cryostat assembly is moved into the airlock of the glove box. (**e**) The cryostat is moved into the glove box from the airlock. (**f**) The cryostat is removed from the vacuum assembly. Pre-cooled forceps are used to position the cryo-shuttle holder on the cryo-moat support after LN2 boils off below its top surface and the cryo-jacket is removed from the cryostat. (**g**) A larger view of the cryo-shuttle holder on the cryo-moat support with the cryo-jacket removed. (**h**) The cryostat is positioned on the lift out station. (**i**) The frost cover is flipped open; a grid carrier is position into the recessed region, and *ex situ* lift out and manipulation can begin.

cleaner for 30 s at 20 mA to aid in Van der Waals adhesion of the cryo-EXLO specimens.

The following manipulator steps were identical for both the polymer and yeast cryo-EXLO and are shown schematically in the diagram in Figure 2. A cryostat was developed for the dual purpose of accepting a cryo-FIB shuttle holder with an anti-frost lid and for the cryo-EXLO. After cryo-FIB milling, the transfer rod was attached to the cryo-shuttle holder, the anti-frost lid was flipped into the closed position, and the cryo-shuttle holder was transferred under vacuum to a gold-coated copper shuttle holder jacket inside the cryostat (Fig. 2a). The rod was removed, and the cryostat assembly was covered and evacuated for transfer to the glove box via an air lock (Fig. 2b). The cryo-jacket keeps the cryo-FIB-milled lift out specimens under cryogenic conditions. This entire transfer process took only seconds to accomplish. This short time for transfer is key to maintain the vitreous specimen at cryogenic conditions as described in Figure 9 and "Thermal Modeling of Cryo-EXLO Specimens" below. Figure 2c shows a top-down view of the cryostat inside the vacuum assembly with the cover removed for clarity. Note the cryo-shuttle holder with anti-frost lid in the closed position and inside the cryo-jacket and the cryo-moat support are positioned for a subsequent transfer step described below. The evacuated assembly is moved to the glove box air lock (Fig. 2d). Note the gloves on the glove box are omitted in this schematic for clarity (Figs. 2d–2f, 2h). The assembly is moved from the air lock and into the glove box (Fig. 2e). The assembly is vented and the cryo-shuttle holder is transferred from the shuttle holder jacket onto a cryo-moat support. The cryo-jacket is no longer needed so it is removed from the cryostat (Fig. 2f). A larger view of the cryo-shuttle holder on the cryo-moat support with the cryo-jacket removed is shown in Figure 2g. The cryostat was positioned on the Nicola 640 lift out station located inside the glove box and the anti-frost lid was opened (Figs. 2h, 2i). Note that for simplicity, the Nicola 640 lift out station is shown without its motor controllers or computer. The cryo-shuttle holder and cryo-moat support in Figure 3 are shown outside of the

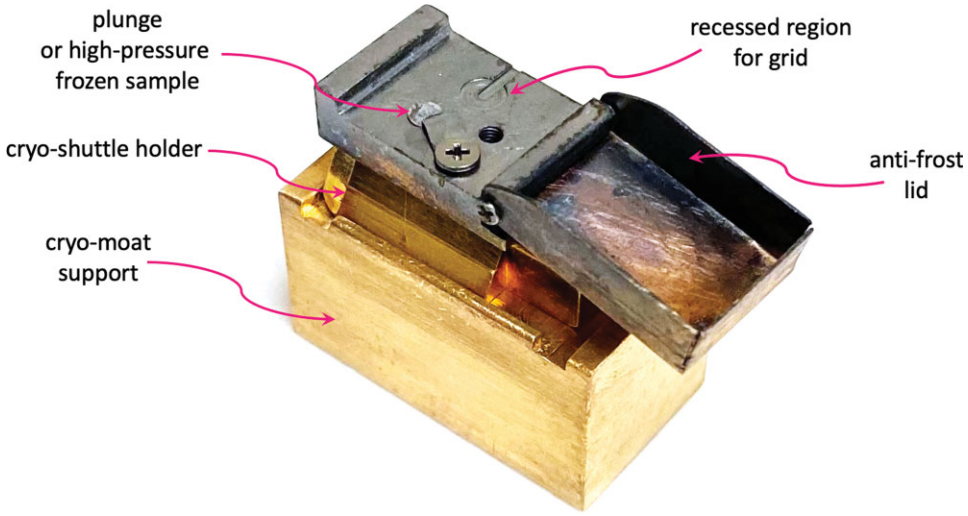

Fig. 3. The cryo-shuttle holder with anti-frost lid shown positioned on the cryo-moat support.

cryostat to illustrate its position. Note that the top of the cryo-shuttle holder is discolored due to the Au–Pd sputter-coating performed inside the Quorum preparation chamber. The anti-frost lid, the predefined positions designed to accept a plunge-frozen grid of yeast cells, and a recessed region for grids or pre-clipped grids are labeled.

The LN2 level in the cryostat was kept just below the working surface of the cryo-shuttle holder to perform cryo-EXLO in the cryogenic vapor phase. A pre-clipped grid and the manipulators were pre-cooled in LN2 just prior to the cryo-EXLO process. The pre-clipped grid was then positioned on the cryo-shuttle holder work surface into its predefined recessed area, and the manipulator probes were positioned for cryo-EXLO as per Figure 2i. Note that once the manipulators are positioned, they remain in the cryogenic vapor phase throughout the lift out and the manipulation process. Once the cryo-shuttle holder was transferred and positioned in the cryostat cryo-moat support on the lift out station, cryo-EXLO was performed nearly identical to ambient EXLO. The major distinction was that the cryo-EXLO process was performed on the cryo-shuttle holder work surface in cryogenic vapor above the LN2 surface. Specific steps and apparatus for cryo-EXLO were designed to reduce ice contamination and to make sure the specimen remained vitreous throughout all steps.

We also performed conjugate conduction-radiation thermal analysis of the FIB specimen geometry and temperature environment. We modeled the geometry of a FIB chamber with Quorum cryo-stage hardware and a FIB-thinned ice specimen inside its trench walls. The details of the modeling will be presented elsewhere, but we include some of the pertinent results below for completeness and validation of the cryo-EXLO method.

Results and Discussion

Cryo-EXLO of Polymer Sample

Figure 4 summarizes the cryo-EXLO steps for the polymer specimen. Figure 4a shows an SEM image of the electron transparent polymer specimen completely FIB milled free and ready for cryo-EXLO. Figure 4b is a light optical micrograph obtained with the Nicola lift out system where the microscope focal plane is at the 3D-printed sample surface. Thus, after cryo-EXLO, the probe containing the manipulated polymer specimen (shown arrowed) is above the 3D-printed sample surface and therefore out of focus. The manipulator probe with the specimen attached is raised about 500 μm to 1 mm to permit stage movement such that the holey-carbon TEM grid is positioned under the probe. The probe with the specimen is then lowered and the specimen is manipulated to the grid, as shown in Figure 4c. Once the specimen is released from the probe, the probe is used to gently pat down the specimen (arrowed in Fig. 4c) to ensure that it remains adhered to the carbon film. The anti-frost cover is closed, the cryostat is covered and removed from the glove box and the grid is cryo-transferred to the autoloader for cryo-TEM. The cryo-EXLO process time between images in Figures 4b, 4c was only about 6 min. It is expected that

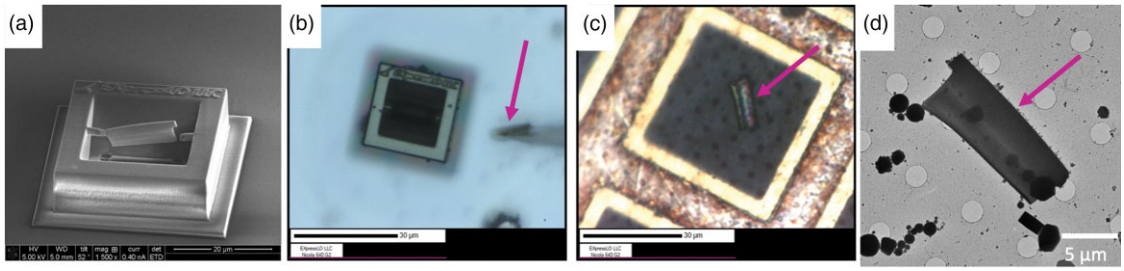

Fig. 4. (**a**) SEM image of cryo-FIB-milled polymer specimen ready for cryo-EXLO. (**b**) Cryo-EXLO of the polymer specimen shown arrowed on the manipulator probe. (**c**) Light optical microscope image from the Nicola system after cryo-EXLO micromanipulation of the polymer specimen onto a carbon-coated (C-Flat) TEM grid. (**d**) Low magnification energy filtered cryo-TEM image of the cryo-EXLO-manipulated polymer specimen.

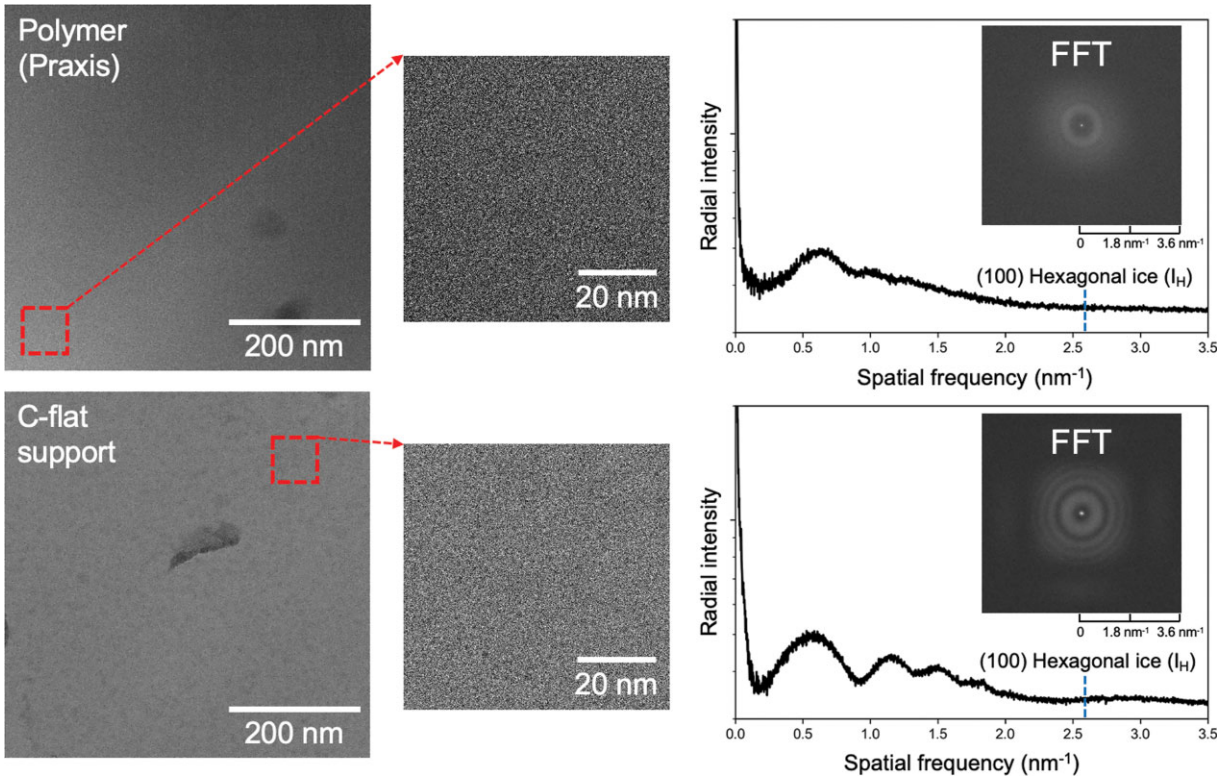

Fig. 5. From left to right: energy filtered cryo-TEM images of the polymer sample and C-flat carbon support film from low to high magnification. Also shown is the radial intensity of the fast Fourier transform (FFT) of each region indicated by the images. Note there is no broad peak at 2.57 nm^{-1} which would indicate ice contamination in the form of hexagonal ice during the cryo-transfer process.

this manipulation time can be significantly reduced with refinement. Figure 4d shows a low magnification cryo-TEM image of the cryo-EXLO-manipulated polymer specimen. While some ice contamination is evident, these artifacts are on par with ice contamination observed in cryo-INLO FIB-prepared specimens. Note there are very large contamination-free regions of the polymer as described in detail below. The successful cryo-EXLO manipulation of a polymer specimen implies that this technique may be used for other materials science applications.

Figure 5 shows energy-filtered cryo-TEM images of the polymer sample and the C-Flat™ carbon support film from low to high magnification. Also shown is the radially integrated intensity as a function of frequency of each fast Fourier transform (FFT) obtained for each region indicated by the images. Note there is no broad peak at 2.57 nm^{-1} which would indicate ice contamination during the cryo-transfer process. Thus, successful cryo-EXLO of a polymer specimen was performed. We expect that cryo-FIB-EXLO can easily be applied to other beam-sensitive materials of interest to physical scientists.

Cryo-EXLO for Vitreous Biological Samples

As shown in the sequence of images in Figure 6, we were able to cryo-FIB, cryo-transfer, and cryo-EXLO manipulate the plunge-frozen yeast, and image the thinned yeast specimen via cryo-TEM. Figures 6a and 6b show SEM images at two different tilt conditions of four cryo-FIB thinned specimens from plunge-frozen yeast cells. All four specimens were FIB milled to electron transparency and were ready for cryo-EXLO in < 4 h. Together with the rapid cryo-EXLO process, the preparation of four complete EXLO-type specimens was therefore significantly faster compared to the typical cryo-INLO approach which requires final thinning steps after the lift out is completed (Parmenter & Nizamudeen, 2021). The yeast cells were cryo-transferred to the lift out station inside the glove box as described above. Figure 6c shows a cryo-EXLO-manipulated light optical microscope (LOM) image of the yeast specimen shown with the arrows in Figures 6a and 6b, and then cryo-EXLO manipulated onto a pre-clipped C-Flat™ carbon support film grid (Fig. 6d) so that it could directly be cryo-transferred into the cryo-TEM sample autoloader cassette. Note that the images in Figures 6c and 6d were acquired with an elapsed time of only ~3.5 min between them. Thus, we were able to reduce the manipulation time between the polymer specimen above (Fig. 4) and the yeast cells (Fig. 6) by nearly a factor of 2×. Since the cryo-TEM was not available until the next morning, we cryo-transferred the grid/autogrid assembly with the cryo-EXLO specimen into LN2 storage and then cryo-transferred the grid/autogrid into the autoloader cassette and cryo-TEM the following day.

Figure 6e shows a low magnification energy filtered cryo-TEM image of cryo-EXLO-manipulated yeast cells. Details of the cryo-TEM results denoted by regions labeled 1, 2, 3, and 4 are described below. As is evident, there is very little ice contamination on the specimen.

To be clear and re-emphasize the EXLO steps—there is NO poking or stabbing of the specimen with the probe. The long axis of the probe is approximately parallel to the specimen lamellae plane, so as the smooth surface of the probe nears the FIB-milled specimen surface, the specimen

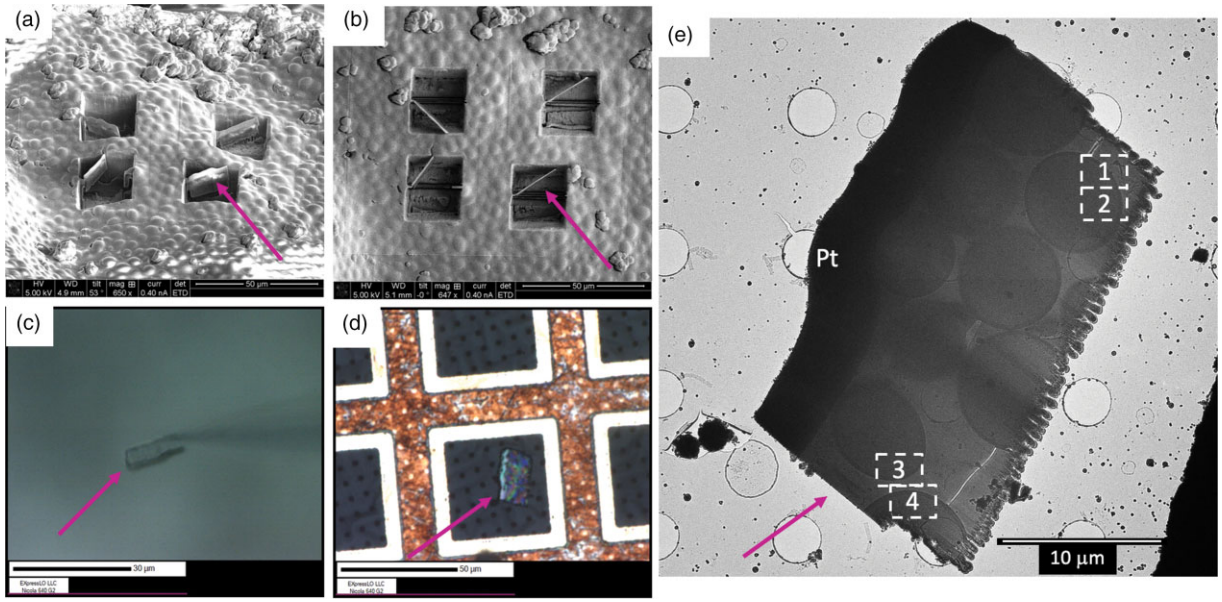

Fig. 6. (**a, b**) SEM images of four cryo-FIB prepared yeast EXLO specimens. (**c**) cryo-EXLO-manipulated yeast specimen arrowed in (**a, b**). (**d**) Light optical micrograph of cryo-EXLO yeast on C-flat grid. (**e**) Low magnification cryo-TEM image of the cryo-FIB-milled and cryo-EXLO-manipulated yeast specimen.

jumps and adheres to the probe via Van der Waals forces. If necessary, the rounded smooth probe tip is used to gently pat down the specimen to ensure that it adheres to the carbon support film. In addition, a second manipulator probe can be used to help with specimen orientation and manipulation as per standard ambient EXLO practice. Thus, as evident, it is possible to manipulate fragile biological cryo-FIB prepared specimens without impaling or inducing physical damage to the specimen.

Figure 7 shows higher resolution energy-filtered cryo-TEM images from regions labeled "1" and "2" in Figure 6e. Note that the yeast cell wall is evident on both images as well as a vesicle within the yeast. The change in mass-thickness contrast running diagonally in Figure 7, number "2" is due to slight FIB curtaining. While noticeable, the curtaining does not alter the results. The FFTs and radial intensity vs. frequency plots from these regions exhibit no evidence of devitrification indicating that the cryo-EXLO process, workflow, and methods function as designed and planned. Cryo-TEM images from regions labeled "3" and "4" from different yeast cells indicated in Figure 6e are detailed in Figure 8. In this case, FFTs did show a trace of a devitrification in the ice region shared between these adjacent yeast cells as evident by the FFTs, radial profile, and Fourier filtered maps. However, the yeast cells show no evidence of crystalline regions, and the results show unambiguously that cryo-EXLO succeeded in keeping the yeast cells vitreous. There is currently no way to tell at what step devitrification of this region occurred, but we plan on extensive research for future assessment of the entire workflow and processes.

Thermal Modeling of Cryo-EXLO Specimens

We modeled the materials, geometry, and properties of a FIB SEM chamber equipped with a Quorum cryo-stage. The simulations include heat transfer due to radiation from the FIB SEM column and the chamber walls, conduction through the walls, the columns, and the sample stage, and convection from the LN2 channels running through the heat conducting cryogenic stage. The LN2 flow was adjusted in the model such that the cryo-stage temperature would reach a temperature between −165°C and −170°C, and the FIB SEM vacuum chamber cold finger was set to ∼−190°C. Figure 9a shows a 100 nm thick ice specimen undercut via a U-shape, only attached via material tabs. Note that the color distribution in Figure 9a represents a total scale of ∼1.3°C with the center of the specimen and material tabs varying by only ∼1°C. This model shows that the specimen remains under cryogenic conditions and below the vitreous temperature of ice (∼−140°C) while LN2 is continuously flowing. These modeling results are consistent with all cryo-FIB work reported to date, i.e., the specimen will remain vitreous while touching another cryogenic surface. Note that for cryo-EXLO, at least one or more specimen surfaces will remain touching a portion of its FIB trench walls (e.g., Figs. 1a, 1b, 4a, 6a, and 6b). Thus, this predicts that a cryo-EXLO FIB-milled specimen will remain vitreous inside its trench indefinitely while LN2 is supplied to the bulk sample shuttle holder. Note that if the cryo-EXLO specimen ceases to touch any trench surface then it is impossible for the specimen to stay in the trench and the specimen will be lost. We note that it is important to use a thick cryo-deposited conductive coating prior to the milling process to prevent charging artifacts that may exceed the Van der Waals forces which keep the specimen in contact with the trench surfaces.

Figure 9b shows a graph of the average specimen temperature (with geometry as per Fig. 9a) as a function of time once the LN2 is turned off. Turning off the LN2 simulates the transfer steps necessary to move the bulk sample shuttle holder between cryogenic conditions (e.g., from the cryo-FIB stage to the cryo-air-lock sub-stage to the cryo-EXLO cryostat and onto the cryo-EXLO moat shuttle holder). The graph in Figure 9b demonstrates that the modeling ice specimen will remain vitreous (< ∼ −140°C) for ∼4.2 min due to thermal conductivity after the LN2 flow stops. This is more than sufficient time to transfer the bulk cryo-shuttle holder from the cryo-FIB stage to the cryo-EXLO cryostat since the transfer step requires only seconds to perform before the cryo-shuttle holder

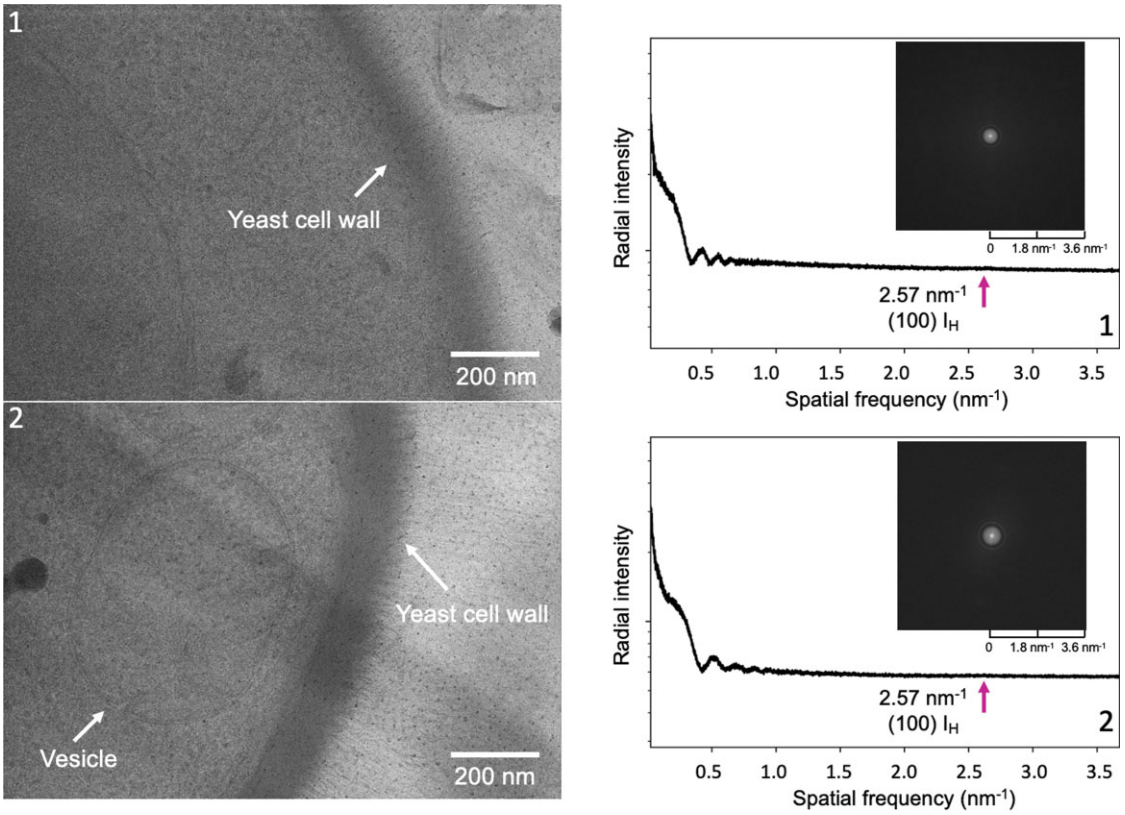

Fig. 7. Cryo-TEM results of cryo-EXLO-manipulated FIB-milled yeast cells. Images, FFTs, and radial frequency plots from regions 1 and 2 (see Fig. 6e) show no evidence of devitrification.

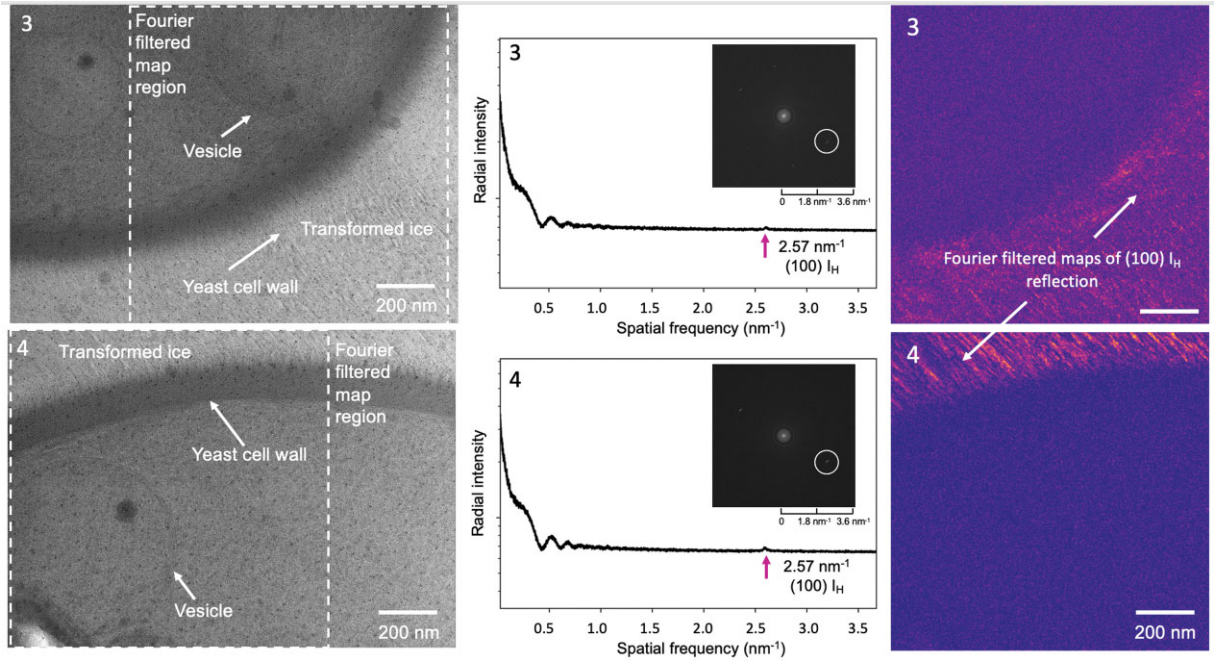

Fig. 8. Cryo-TEM results of cryo-EXLO-manipulated FIB-milled yeast cells. Images, FFTs, radial frequency plots, and FFT maps from regions 3 and 4 (Fig. 6e) show evidence of devitrification in the ice between yeast cells.

is again cooled with LN2 by the cryo-jacket within the cryo-stat, and from the cryo-jacket to the cryo-moat. Thus, the heat transfer model demonstrates that the cryo-EXLO process allows the specimen to remain at or colder than vitreous conditions during all FIB milling and cryo-transfers steps. These thermal modeling results support the cryo-TEM experimental results showing that cryo-FIB milling and cryo-EXLO manipulation are possible.

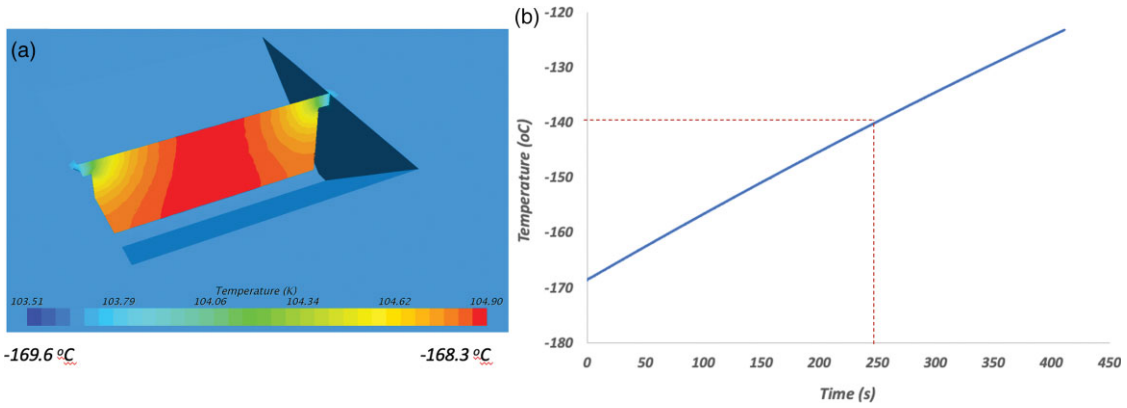

Fig. 9. (**a**) A 100 nm thick ice specimen attached via material tabs to its trench walls with continuous LN2 flowing. (**b**) Ice specimen warming as a function of time with LN2 flow turned off.

Conclusions

This work describes a method of cryo-EXLO for cryo-FIB-thinned specimens for analysis by cryo-TEM. It should be appreciated that these site-specific cryo-EXLO-manipulated specimens can be analyzed by other cryo-characterization techniques. The transfer steps and apparatus necessary for cryo-EXLO from the cryo-FIB to the cryo-TEM were described in detail. We designed methods and apparatus to limit ice contamination including the use of an anti-frost lid, a cryostat during cryo-EXLO, and a vacuum transfer assembly for all cryo-shuttle holder transfer steps. To avoid ice contamination and maintain the vitreous phase of specimens, cryo-EXLO is performed in a cryostat with the cryo-shuttle holder positioned in the cryogenic vapor phase above the surface of liquid N_2 (LN2) using an EXLO manipulation station installed inside a glove box maintained at < 10% relative humidity and inert (e.g., N_2 gas) conditions. Thermal modeling showed that a cryo-EXLO specimen will remain at cryogenic temperatures indefinitely while confined to its FIB trenches while LN2 is continuously supplied to its bulk cryo-shuttle holder. Once the LN2 is cut off, modeling shows that the EXLO specimen in its trench will warm slowly, remaining vitreous for over 4 min, allowing more than sufficient time for the cryo-transfer steps which take only seconds to perform. Cryo-EXLO was applied successfully to cryo-FIB-milled specimens prepared from a polymer and plunge-frozen yeast cells. Cryo-TEM of both the polymer and the yeast showed minimal ice contamination. The yeast maintained its vitreous phase from cryo-FIB to cryo-EXLO to cryo-TEM. Future work will include cryo-tomography of yeast and other materials via cryo-EXLO methods. In particular, we plan on applying cryo-EXLO for cryo-TEM tomography using high-pressure frozen samples. These results show the potential of cryo-EXLO for cryo-FIB-EM of beam-sensitive, liquid, or biological materials.

Acknowledgments

Thanks to K. Scott at NIST for providing an extra cryo-stage for testing. Thanks to R. Stephano for help with machining. Thanks to R. Joseph for help with software development. Thanks to T. Dougherty for providing CAD figures. Thanks to A. Dohnalkova for helpful discussions. The cryo-EXLO methods and apparatus are patent-pending.

Conflict of interest

The authors declare that they have no competing interest.

Financial support

This work was supported by DOE BER award DE-SC0020511. Additional support was provided by NSF (DMR-1654596, DMR-1429155). This work made use of the Cornell Center for Materials Research Shared Facilities which are supported through the NSF MRSEC program (DMR-1719875).

References

Antoniou N, Graham A, Hartfield C & Amador G (2012). Failure analysis of electronic material using cryogenic FIB-SEM. In Conference Proceedings from the 38th International Symposium for Testing and Failure Analysis, Phoenix, AR, November 11–15, 2012, pp. 399–405. ASM International.

Choudhury S, Tu Z, Nijamudheen A, Zachman MJ, Stalin S, Deng Y, Zhao Q, Vu D, Kourkoutis LF, Mendoza-Cortes JL & Archer LA (2019). Stabilizing polymer electrolytes in high-voltage lithium batteries. *Nat Commun* **10**(1), 3091.

Doubochet J & McDowall AW (1981). Vitrification of pure water for electron microscopy. *J. Microsc* **124**(3), 3–4.

Ferryman AC, Fulghum JE, Giannuzzi LA & Stevie FA (2002). XPS analysis of Si samples prepared by the FIB lift-out technique. *Surf Interface Anal* **33**(12), 907–913.

Ghassemi H, Jacobs B, Asayesh-Ardakani H, Yao W, Giannuzzi LA & Shahbazian-Yassar R (2017). Simultaneous structural and electrical analysis of vanadium dioxide using in situ TEM. *Microsc Microanal* **23**(Suppl 1), 1672–1673.

Giannuzzi LA (2017). Optimizing ex situ Lift Out for Frontside or Backside FIB Milling. In ISTFA 2017: Proceedings from the 43rd International Symposium for Testing and Failure Analysis, Pasadena, CA, November 5–9, 2017, pp. 275. ASM International.

Giannuzzi LA, DeVore M, Summer M & Wellons M (2019*a*). Micromanipulation, FIB, STEM, EDS and EELS of UF 4 particles. *Microsc Microanal* **25**(Suppl 2), 1584–1585.

Giannuzzi LA, Drown JL, Brown SR, Irwin RB & Stevie FA (1997). Focused ion beam milling and micromanipulation lift-out for site specific cross-section TEM specimen preparation. In *Workshop on Specimen Preparation for TEM of Materials IV. Material Research Society Symposium Proceedings*, Anderson RM & Walck SD. (Eds.), pp. 19–27. San Francisco: MRS.

Giannuzzi LA, Harrison SL, Williams KL, Goduguchinta RK, Vaaler EG, Schneiter JL & Pegna J (2016). Manipulation of ceramic fibers

to EXpressLO™ grids for FIB/TEM analysis. *Microsc Microanal* **22**-(Suppl 3), 134–135.

Giannuzzi LA, Kempshall BW, Schwarz SM, Lomness JK, Prenitzer BI & Stevie FA (2005). FIB lift-out specimen preparation techniques: Ex-situ and in-situ methods. In *Introduction to Focused Ion Beams: Instrumentation, Theory, Techniques, and Practice*, Giannuzzi LA & Stevie FA (Eds.), pp. 201–228. New York: Springer.

Giannuzzi LA & Stevie FA (1999). A review of focused ion beam milling for TEM specimen preparation. *Micron* **30**, 197–204.

Giannuzzi LA, Yu Z, Yin D, Harmer MP, Xu Q, Smith NS, Chan L, Hiller J, Hess D & Clark T (2015). Theory and new applications of ex situ lift out. *Microsc Microanal* **21**(4), 1034–1048.

Giannuzzi ZA, Giannuzzi LA, Gehoski KA & Mahoney WJ (2019*b*). 3D-printed samples for EXLO/INLO practice and training. In ISTFA 2019: Proceedings of the 45th International Symposium for Testing and Failure Analysis, Portland, OR, November 10–14, 2019, pp. 236–240. ASM International.

Giddings TH, O'Toole ET, Morphew M, Mastronarde D, McIntosh JR & Winey M (2001). Using rapid freeze and freeze-substitution for the preparation of yeast cells for electron microscopy and three-dimensional analysis. *Methods Cell Biol* **67**, 27–42.

Hayles MF, Stokes DJ, Phifer D & Findlay KC (2007). A technique for improved focused ion beam milling of cryo-prepared life science specimens. *J Microsc* **226**(3), 263–269.

Heymann JAW, Hayles M, Gestmann I, Giannuzzi LA, Lich B & Subramaniam S (2006). Site-specific 3D imaging of cells and tissues with a dual beam microscope. *J Struct Biol* **155**(1), 63–73.

Hsieh C, Schmelzer T, Kishchenko G, Wagenknecht T & Marko M (2014). Practical workflow for cryo focused-ion-beam milling of tissues and cells for cryo-TEM tomography. *J Struct Biol* **185**, 32–41.

Klumpe S, Fung HK, Goetz SK, Zagoriy I, Hampoelz B, Zhang X, Erdmann PS, Baumbach J, Müller CW & Beck M (2021). A modular platform for automated cryo-FIB workflows. *Elife* **10**, e70506.

Ladinsky MS (2010). Micromanipulator-assisted vitreous cryosectioning and sample preparation by high-pressure freezing. In *Cryo-EM Part A: Sample Preparation and Data Collection. Methods in Enzymology*, Jensen G (Ed.), pp. 211–240. San Diego: Academic Press.

Li YZ, Li YB & Cui Y (2018). Catalyst: how cryo-EM shapes the development of next-generation batteries. *Chem* **4**(10), 2250–2252.

Marko M, Hsieh C, Moberlychan W, Mannella CA & Frank J (2006). Focused ion beam milling of vitreous water: Prospects for an alternative to cryo-ultramicrotomy of frozen-hydrated biological samples. *J. Microsc* **222**, 42–47.

Parmenter CDJ, Fay MW, Hartfield C & Eltaher HM (2016). Making the practically impossible "merely difficult"—cryogenic FIB lift-out for "damage free" soft matter imaging. *Microsc Res Tech* **79**, 298–303.

Parmenter CD & Nizamudeen ZA (2021). Cryo-FIB-lift-out: practically impossible to practical reality. *J Microsc* **281**(2), 157–174.

Rigort A, Bäuerlein FJB, Villa E, Eibauer M, Laugks T, Baumeister W & Plitzko JM (2012). Focused ion beam micromachining of eukaryotic cells for cryoelectron tomography. *Proc Nat Acad Sci USA* **109**, 4449–4454.

Rubino S, Akhtar S, Melin P, Searle A, Spellward P & Leifer K (2012). A site-specific focused-ion-beam lift-out method for cryo transmission electron microscopy. *J Struct Biol* **180**, 572–576.

Schaffer M, Pfeffer S, Kleindiek S, Mahamid J, Heymann J, Smith AJ, Laugks T, Engel BD, Albert S, Baumeister W & Plitzko JM (2018). Cryo-FIB lamella milling: A comprehensive technique to prepare samples of both plunge- and high-pressure frozen-hydrated specimens for in situ studies. *Microsc Microanal* **24**(1), 820–821.

Schaffer M, Pfeffer S, Mahamid J, Kleindiek S, Laugks T, Albert S, Engel BD, Rummel A, Smith AJ, Baumeister W & Plitzko JM (2019). A cryo-FIB lift-out technique enables molecular-resolution cryo-ET within native *Caenorhabditis elegans* tissue. *Nat Methods* **16**(8), 757–762.

Stevie FA, Vartuli CB, Giannuzzi LA, Shofner TL, Brown SR, Rossie B, Hillion F, Mills RH, Antonell M, Irwin RB & Purcell BM (2001). Application of focused ion beam lift-out specimen preparation to TEM, SEM, STEM. AES and SIMS analysis. *Surf Interface Anal* **31**(5), 345–351.

Zachman MJ, Noble JM & Kourkoutis LF (2017). Cryo-FIB milling and lift-out for preparation of specimens for cryo-TEM. *Micros Microanal* **23**(1), 2312–2313.

Zachman MJ, Zhengyuan T, Choudery S, Archer LA & Kourkoutis LF (2018). Cryo-STEM mapping of solid–liquid interfaces and dendrites in lithium-metal batteries. *Nature* **560**, 345–349.